Title
Coherent control with optical pulses for deterministic spin-photon entanglement

Journal
Physical Review B, 88(19)

ISSN
2469-9950

Authors
Truex, Katherine
Webster, LA
Duan, L-M
et al.

Publication Date
2013-11-15

DOI
10.1103/physrevb.88.195306

Peer reviewed

Coherent control with optical pulses for deterministic spin-photon entanglement

Katherine Truex,[1,*] L. A. Webster,[1] L.-M. Duan,[1] L. J. Sham,[2] and D. G. Steel[1,†]
[1]*The H. M. Randall Laboratory of Physics, The University of Michigan, Ann Arbor, Michigan 48109, USA*
[2]*Department of Physics, The University of California, San Diego, La Jolla, California 92093-0319, USA*
(Received 28 December 2012; published 18 November 2013)

We present a procedure for the optical coherent control of quantum bits within a quantum dot spin-exciton system, as a preliminary step to implementing a proposal by Yao, Liu, and Sham [Phys. Rev. Lett. **95**, 030504 (2005)] for deterministic spin-photon entanglement. The experiment proposed here utilizes a series of picosecond optical pulses from a single laser to coherently control a single self-assembled quantum dot in a magnetic field, creating the precursor state in 25 ps with a predicted fidelity of 0.991. If allowed to decay in an appropriate cavity, the ideal precursor superposition state would create maximum spin-photon entanglement. Numerical simulations using values typical of InAs quantum dots give a predicted entropy of entanglement of 0.929, largely limited by radiative decay and electron spin flips.

DOI: 10.1103/PhysRevB.88.195306 PACS number(s): 03.67.Bg, 78.47.jh, 78.67.Hc

I. INTRODUCTION

The optical manipulation of spins in semiconductor quantum dots is now a mature field, due to the possibility of exploiting long spin coherence times for stable quantum bits (qubits) for quantum computing. Benjamin, Ramsey, and Warburton provide reviews of the achievements in the field.[1–3] Recent experiments, since 2010, have demonstrated optical control of exciton[4] and biexciton[5] generation, as well as control of the spin state of electrons,[6–8] holes,[9,10] and excitons[11–14] in single InAs quantum dots. Efforts continue to better characterize semiconductor quantum dots, including improved understanding of the effects of electric[15,16] and magnetic[17] fields, further studies of the energy levels,[18,19] room-temperature studies,[20] and many other critical measurements.[21–26] Several groups demonstrated new spin readout methods,[27–29] addressing one of DiVincenzo's criteria for quantum computing.[30] Impressive progress has been made recently in characterizing and manipulating InAs quantum dot molecules,[28,31–36] including demonstration of two-qubit gates.[37]

A necessary next step for quantum dot based quantum computing is to extend such results to many-qubit systems.[30] A quantum computer that is complex enough to solve interesting problems will require many qubits and would be overly complex if a large number of qubits were unavoidably and simultaneously coupled. To address this problem, we adopt the strategy of the quantum network.[38,39] Yao, Liu, and Sham (YLS) have suggested a network of spin qubits in quantum dots that can exchange information by means of a flying photon qubit. Specifically, a flying photon qubit that is entangled with one stationary spin qubit could be used to produce entanglement with a second spatially separated qubit.[40] There have been several recent demonstrations of entanglement of quantum dot spins and photons.[41–43] However, these experiments depend on the stochastic spontaneous radiation from an optically excited state, whereas the proposal by YLS to entangle the flying photon qubit with the stationary spin qubit in a quantum dot is deterministic. Here, we suggest and analyze a scheme for achieving this controlled photon-spin entanglement using the spin of an electron confined in an InAs quantum dot (energy level diagram in Fig. 1).

The YLS proposal places the quantum dot in an appropriately designed photonic cavity such that the Purcell effect modifies the spontaneous emission rates to suppress emission along the $|T_+\rangle$ to $|x_-\rangle$ transition while augmenting emission along the $|T_+\rangle$ to $|x_+\rangle$ transition.[44,45] In this system, the electron spin is the qubit, and its two states are given in the x basis. Any arbitrary coherent superposition state of the electron spin in the absence of cavity photons can be written in the field interaction picture[46] as $(\alpha|x_-\rangle + \beta|x_+\rangle)|0\rangle_c$, where α and β may be complex and $|0\rangle_c$ represents an empty cavity mode. If this quantum state were coherently transformed into the state $|\Psi^E\rangle = (\alpha e^{i\phi_\alpha}|x_-\rangle + \beta e^{i\phi_\beta}|T_+\rangle)|0\rangle_c \equiv |\psi^E\rangle|0\rangle_c$ and then allowed to radiatively decay, the resulting state of the dot-cavity system would be $(\alpha e^{i\Phi_\alpha}|x_-\rangle|0\rangle_c + \beta e^{i\Phi_\beta}|x_+\rangle|1\rangle_c)$, where $|1\rangle_c$ represents the presence of a photon in the cavity mode, and ϕ and Φ are constant phases accumulated during the transformations. This scheme forms an entanglement between the spin state of the electron and the presence or absence of a cavity photon. The transformation of an arbitrary spin state into state $|\Psi^E\rangle$ is thus a preliminary step to photon-spin entanglement. We describe and analyze a procedure for this transformation and for the creation of $|\psi^E\rangle$ in a single InAs quantum dot in commonly studied samples that do not contain photonic cavities as groundwork for eventual demonstrations with photonic cavity samples.

The YLS protocol requires being able to create an arbitrary superposition of the two spin states and then selectively exciting one of the spin states ($|x_+\rangle$) to the trion state ($|T_+\rangle$) with unity probability. In principle, a polarized narrow-bandwidth optical pulse would excite the $|x_+\rangle$ to $|T_+\rangle$ transition, but not any other transition. However, a short pulse is needed to limit the decoherence and hence to maximize the fidelity of the spin photon entanglement. Additionally, the pulse area[47] must be π, placing a power requirement on the system. Since a short pulse will also excite the $|T_-\rangle$ state, we propose an alternate method for selective excitation using the composite properties of two phase-locked pulses[48] that are readily available from commonly used lasers.

The organization of the remainder of the paper is as follows. In Sec. II, we detail the selective excitation of an arbitrary state

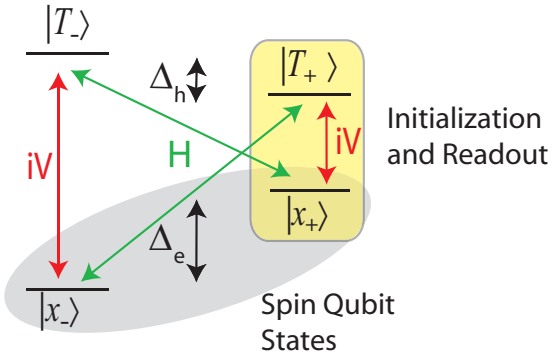

FIG. 1. (Color online) Lowest energy levels and allowed optical transitions for a charged InAs quantum dot in a Voigt geometry magnetic field (with the magnetic field along $\hat{\mathbf{x}}$ and perpendicular to the growth direction, $\hat{\mathbf{z}}$). The two ground states, $|x_-\rangle$ and $|x_+\rangle$, represent the two spin states of an electron energetically confined in the dot, with the direction defined relative to the magnetic field. These are the states of the spin qubit. States $|T_-\rangle$ and $|T_+\rangle$ are the optically excited states (trions), which are quasiparticles composed of two spin-paired electrons and a hole. In this case, the sign indicates the spin orientations of the hole along the magnetic field direction. Δ_e and Δ_h are the electron and hole Zeeman splitting frequencies, respectively. In typical samples, the optical resonance that couples the electron ground state and first excited state is around 950 nm, and in a 5.5 T magnetic field $\Delta_e = 30$ GHz and $\Delta_h = 20$ GHz. V and H indicate that the allowed optical transition between two states is vertically or horizontally polarized, as labeled, and the i indicates a phase difference between the transition dipole moments.

of the spin qubit to the state $|\psi^E\rangle$ with two phase-coherent, picosecond, on-resonance pulses. In Sec. III, we describe a complete experimental procedure for producing and detecting $|\psi^E(t)\rangle$. Section III concludes by discussing measurement of the coherence of $|\psi^E(t)\rangle$ using a fifth pulse and the absorption of the CW laser. Lastly, in Sec. IV we present the results of numerical simulations using typical experimental values, which predict the fidelity and entropy of entanglement that the proposed experiment should create.

II. SELECTIVE EXCITATION BY A PULSE PAIR

This section details how two picosecond pulses can coherently transform an arbitrary spin state $\alpha|x_-\rangle + \beta|x_+\rangle$ in an InAs quantum dot to state $|\psi^E\rangle$. The method presented here avoids unintended dynamics associated with level $|T_-\rangle$ and creates a state that can persist for a time limited only by decay and decoherence. This discussion illustrates the basic physical behavior, which we label "selective excitation," made possible with phase-locked pulses. This physical behavior is essential for a successful outcome of the complete experimental design in Sec. III. A recent paper demonstrates the viability of this pulse shaping method in InAs quantum dots.[49]

The goal of the following development is to obtain an analytical expression for the state of a quantum dot after excitation by two on-resonant optical pulses. Specifically, we define two identical pulses that arrive at the sample at times t_a and t_b, such that the incident electric field associated with the

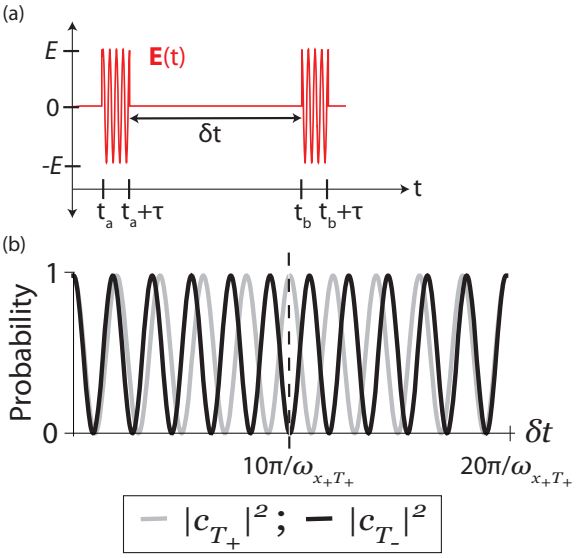

FIG. 2. (Color online) (a) A graph of the electric field for the two square pulses defined in Eq. (1). (b) The probabilities that a dot with $|c_{x_-}(t_a)|^2 = |c_{x_+}(t_a)|^2 = 0.5$ would be in states $|T_+\rangle$ and $|T_-\rangle$ after two optical pulses as defined in Eq. (1) with pulse area $\theta = |\Omega|\tau = \pi/2$. The probabilities are calculated using Eq. (8) and plotted as a function of delay between the pulses. The dotted line shows the point where $\delta t = \pi/(\omega_{x_-T_-} - \omega_{x_+T_+})$ and $(\delta t + \tau)\omega_L = \pi/2$. At this delay, the transitions $|x_+\rangle$ to $|T_+\rangle$ and $|x_-\rangle$ to $|T_-\rangle$ are exactly out of phase. Recall the laser frequency, ω_L, is set such that $\omega_L = (\omega_{x_-T_-} + \omega_{x_+T_+})/2$. For this plot, $\omega_{x_-T_-} = 1.1\omega_{x_+T_+}$ in order to illustrate a visible phase difference within a few periods. Typical experimental values for a 5.5 T magnetic field are $\omega_{x_-T_-} = 1.00016\omega_{x_+T_+}$.

optical pulses is

$$\mathbf{E}(t) = E\hat{\mathbf{y}} \sqcap \left(\frac{t - t_a}{\tau}\right) \cos[\omega_L(t - t_a) + \phi] + E\hat{\mathbf{y}} \sqcap \left(\frac{t - t_b}{\tau}\right) \cos[\omega_L(t - t_b) + \phi], \quad (1)$$

where τ is the pulse width, the relative phase between the pulse envelope and the optical carrier is ϕ, and $\sqcap(t/\tau)$ is defined as

$$\sqcap\left(\frac{t}{\tau}\right) = \begin{cases} 1 & \text{if } 0 \leqslant t < \tau, \\ 0 & \text{if } t < 0 \text{ or } t \geqslant \tau. \end{cases} \quad (2)$$

$\mathbf{E}(t)$ is plotted in Fig. 2(a). We can approximate the pulses as square in shape (with constant amplitudes) since we are interested only in the state of the dot after the excitation and since the pulse widths are short compared to all relaxation times in the system. If both pulses are vertically polarized, as indicated by the unit vector $\hat{\mathbf{y}}$, then only the $|x_+\rangle$ to $|T_+\rangle$ and the $|x_-\rangle$ to $|T_-\rangle$ transitions will be excited, as illustrated in Fig. 1. These two transitions have different frequencies $\omega_{x_+T_+}$ and $\omega_{x_-T_-}$ due to the Zeeman splittings. For selective excitation, the center frequency of both pulses is tuned to halfway between the $|x_+\rangle$ to $|T_+\rangle$ and the $|x_-\rangle$ to $|T_-\rangle$ transition frequencies $[\omega_L = (\omega_{x_+T_+} + \omega_{x_-T_-})/2]$.

A complete expression for the time dependence of the state of the dot would include decay and decoherence effects, which generally require the use of density matrix notation.[46] However, since the pulse widths and time between pulses are

short compared to the decay and decoherence times, these effects can be neglected when calculating the state of the dot following the pulses. This enables the use of the amplitude picture, where the state of the dot (in the Schrödinger picture) $|\psi\rangle = a_{x_-}|x_-\rangle + a_{x_+}|x_+\rangle + a_{T_+}|T_+\rangle + a_{T_-}|T_-\rangle$ is described by the time-dependent probability amplitudes, $a_i(t)$.

The effect of these optical pulses on a dot is most simply described in the field interaction picture,[46] defined as

$$\mathbf{c}(t) = \begin{bmatrix} e^{i\omega_L t/2} & 0 & 0 & 0 \\ 0 & e^{i\omega_L t/2} & 0 & 0 \\ 0 & 0 & e^{-i\omega_L t/2} & 0 \\ 0 & 0 & 0 & e^{-i\omega_L t/2} \end{bmatrix} \mathbf{a}(t) \tag{3}$$

for optical excitation at frequency ω_L.

The equations of motion for the probability amplitudes in the field interaction representation and the rotating wave approximation are

$$\begin{aligned} \dot{c}_{x_-}(t) &= i\left[\pi\Delta_e c_{x_-}(t) - \frac{\Omega^*}{2}c_{T_-}(t)\right], \\ \dot{c}_{x_+}(t) &= i\left[-\pi\Delta_e c_{x_+}(t) - \frac{\Omega^*}{2}c_{T_+}(t)\right], \\ \dot{c}_{T_+}(t) &= i\left[-\frac{\Omega}{2}c_{x_+}(t) + \pi\Delta_h c_{T_+}(t)\right], \\ \dot{c}_{T_-}(t) &= i\left[-\frac{\Omega}{2}c_{x_-}(t) - \pi\Delta_h c_{T_-}(t)\right]. \end{aligned} \tag{4}$$

These equations apply for a vertically polarized optical excitation at frequency ω_L. Notice that these equations describe two completely decoupled two-level systems. From the definition of $\mathbf{E}(t)$ in Eq. (1), the Rabi frequency Ω is $-\mu_y E e^{-i(\phi-\omega_L t_a)}/\hbar$ during the first pulse $[t_a \leqslant t < (t_a+\tau)]$, $-\mu_y E e^{-i(\phi-\omega_L t_b)}/\hbar$ during the second pulse $[t_b \leqslant t < (t_b+\tau)]$, and 0 for all other times. $\mu_{T_-x_-}$ is the dipole moment for the transition from state $|T_-\rangle$ to state $|x_-\rangle$. When the transition dipole moments are evaluated using the Wigner-Eckart theorem and known properties of the valence and conduction bands of InAs dots,[50–52] we find that $\mu_{T_-x_-} = \mu_{T_+x_+} \equiv \mu_y$ and $\mu_y^* = -\mu_y$ while $\mu_{T_-x_+} = \mu_{T_+x_-} \equiv \mu_x$ and $\mu_x^* = \mu_x$. The relation $\mu_y = i\mu_x$ leads to a phase difference between the horizontal and vertical transitions.

The probability amplitudes of the dot after the pair of pulses defined by Eq. (1) can be calculated from the product of three matrices, one representing each pulse and one for the time evolution between the pulses. Between the pulses, $\Omega = 0$, which reduces Eq. (4) to four uncoupled equations. The solution for the probability amplitudes of the dot after a time δt without pulses is $\mathbf{c}(t+\delta t) = \mathbf{T}(\delta t)\mathbf{c}(t)$, where

$$\mathbf{T}(\delta t) = \begin{bmatrix} e^{i\pi\Delta_e\delta t} & 0 & 0 & 0 \\ 0 & e^{-i\pi\Delta_e\delta t} & 0 & 0 \\ 0 & 0 & e^{i\pi\Delta_h\delta t} & 0 \\ 0 & 0 & 0 & e^{-i\pi\Delta_h\delta t} \end{bmatrix}. \tag{5}$$

The matrix $\mathbf{T}$ defines the time evolution of the dot in the absence of an optical field, which consists of spin precession due to the magnetic field.

The equations of motion during a pulse can be solved for a simple transition matrix that describes the action of a pulse on the dot. In typical InAs dots, $1/\tau >> \Delta_e, \Delta_h >> \Gamma_T$, where Γ_T is the radiative decay rate of the trion states and determines their natural linewidths. Since the pulse bandwidth is much greater than the state linewidth and the Zeeman splittings, we can ignore the small effect of detuning during the pulse and approximate the optical field as on-resonance with all four optical transitions. The probability amplitudes after a single vertically polarized pulse of pulse width τ are $\mathbf{c}(t+\tau) = \mathbf{P}(\Omega,\tau)\mathbf{c}(t)$, where

$$\mathbf{P}(\Omega,\tau) = \begin{bmatrix} \cos\frac{|\Omega|\tau}{2} & 0 & 0 & -\frac{i\Omega^*}{|\Omega|}\sin\frac{|\Omega|\tau}{2} \\ 0 & \cos\frac{|\Omega|\tau}{2} & -\frac{i\Omega^*}{|\Omega|}\sin\frac{|\Omega|\tau}{2} & 0 \\ 0 & -\frac{i\Omega}{|\Omega|}\sin\frac{|\Omega|\tau}{2} & \cos\frac{|\Omega|\tau}{2} & 0 \\ -\frac{i\Omega}{|\Omega|}\sin\frac{|\Omega|\tau}{2} & 0 & 0 & \cos\frac{|\Omega|\tau}{2} \end{bmatrix}. \tag{6}$$

The probability amplitudes immediately after the two pulses defined by Eq. (1) can now be written as

$$\mathbf{c}(t_b+\tau) = \mathbf{P}\left(-\frac{\mu_y E}{\hbar}e^{-i(\phi-\omega_L t_b)},\tau\right)\mathbf{T}(\delta t)\mathbf{P}\left(-\frac{\mu_y E}{\hbar}e^{-i(\phi-\omega_L t_a)},\tau\right)\mathbf{c}(t_a). \tag{7}$$

As illustrated in Fig. 2(a), $\delta t = t_b - t_a - \tau$. If the system is in a coherent superposition of the ground states when the first pulse arrives such that $c_{T_-}(t_a) = c_{T_+}(t_a) = 0$, then the probabilities after the second pulse simplify to

$$\begin{aligned} |c_{x_-}(t_b+\tau)|^2 &= |c_{x_-}(t_a)|^2\left(1 - \sin^2|\Omega|\tau\cos^2\frac{\omega_{x_-T_-}\delta t + \omega_L\tau}{2}\right), \\ |c_{x_+}(t_b+\tau)|^2 &= |c_{x_+}(t_a)|^2\left(1 - \sin^2|\Omega|\tau\cos^2\frac{\omega_{x_+T_+}\delta t + \omega_L\tau}{2}\right), \\ |c_{T_+}(t_b+\tau)|^2 &= |c_{x_+}(t_a)|^2\left(\sin^2|\Omega|\tau\cos^2\frac{\omega_{x_+T_+}\delta t + \omega_L\tau}{2}\right), \\ |c_{T_-}(t_b+\tau)|^2 &= |c_{x_-}(t_a)|^2\left(\sin^2|\Omega|\tau\cos^2\frac{\omega_{x_-T_-}\delta t + \omega_L\tau}{2}\right), \end{aligned} \tag{8}$$

where

$$\omega_{x-t-} = \omega_L + \pi(\Delta_e + \Delta_h), \quad \omega_{x+t+} = \omega_L - \pi(\Delta_e + \Delta_h), \tag{9}$$

the pulse area θ is $|\Omega|\tau = |\mu_y E|\tau/\hbar$, and time $t = t_a$ is defined as immediately before the first of the two selective excitation pulses.

Equation (8) shows that the delay between the two pulses, δt, determines whether the physical effects driven by the two nonoverlapping pulses combine constructively or destructively. Changes in δt on the order of the optical period of the laser cause the probability at time $t_b + \tau$ to oscillate between states $|x_-\rangle$ and $|T_-\rangle$ at a different rate than between states $|x_+\rangle$ and $|T_+\rangle$. The $|x_+\rangle$ to $|T_+\rangle$ and the $|x_-\rangle$ to $|T_-\rangle$ transitions are precisely out of phase at the delay $\delta t = \pi/(\omega_{x_-T_-} - \omega_{x_+T_+}) = [2(\Delta_e + \Delta_h)]^{-1}$. Because $\omega_L \gg \pi(\Delta_e + \Delta_h)$, we can add a small correction, t_c, to δt such that $(\delta t + \tau)\omega_L = \pi/2$, while not significantly changing terms like $\delta t\pi(\Delta_e + \Delta_h)$. At this delay the pulses will add constructively (destructively) along $|x_+\rangle$ to $|T_+\rangle$ ($|x_-\rangle$ to $|T_-\rangle$), leaving the system in $|\psi^E\rangle$. This effect can only be observed if the delay between the pulses is on the order of the inverse optical frequency.

Figure 2 plots the probabilities for the trion states after the second pulse, $|c_{T_+}(t_b + \tau)|^2$ and $|c_{T_-}(t_b + \tau)|^2$, as expressed by Eq. (8) to illustrate how the relative phase between the two probabilities depends on the delay between the two pulses. The phase of each transition oscillates at the optical transition frequency, but the two transitions move in and out of phase with each other at the slower rate $(\Delta_e + \Delta_h)$. The optimum delay for selective excitation is indicated by the dotted line. To make the phase evolution easier to observe, the difference between the frequencies is enhanced in the figure. For typical Zeeman splittings and a 5.5 T magnetic field, a delay of $\delta t = 10$ ps is optimal for selective excitation and creating the state $|\psi^E\rangle$.

Figure 3 illustrates the selective excitation caused by an appropriately timed pair of pulses. Due to the vertical polarization of the pulse pair, the four-level system simplifies to two decoupled two-level systems, each represented by a Bloch sphere. Before the pulse pair, the dot is in a superposition of the ground states $\alpha|x_-\rangle + \beta|x_+\rangle$. The magnitudes of α and β simply scale the relative size of the two Bloch spheres. To create the desired state $|\psi^E\rangle$, both pulses should have pulse area $\pi/2$. The initial pulse creates a coherent superposition of the four states, which is represented by a rotation of both Bloch vectors by 90°. Between pulses, the Bloch vectors precess in the equatorial plane by angles that correspond to the accumulated phases. These phases have the form $e^{i(\omega_{x_-T_-} - \omega_L)\delta t}$ and $e^{i(\omega_{x_+T_+} - \omega_L)\delta t}$ since the Bloch sphere is defined in the field interaction picture.[46] Since $\omega_L = (\omega_{x_+T_+} + \omega_{x_-T_-})/2$, the two Bloch vectors precess in opposite directions. If the pulses are separated by $\delta t = \pi/(\omega_{x_-T_-} - \omega_{x_+T_+})$, then the difference in accumulated phase is π and the two vectors are pointing in opposite directions when the second pulse arrives. If $(\delta t + \tau)\omega_L = \pi/2$, then the second pulse rotates the Bloch vectors about an orthogonal axis compared to the first pulse. Because the two Bloch vectors are pointing in opposite directions when the second pulse arrives, the second 90° rotation leaves one vector in the ground state and the other vector in the trion state. Thus, after the second pulse the dot is in state $|\psi^E\rangle$.

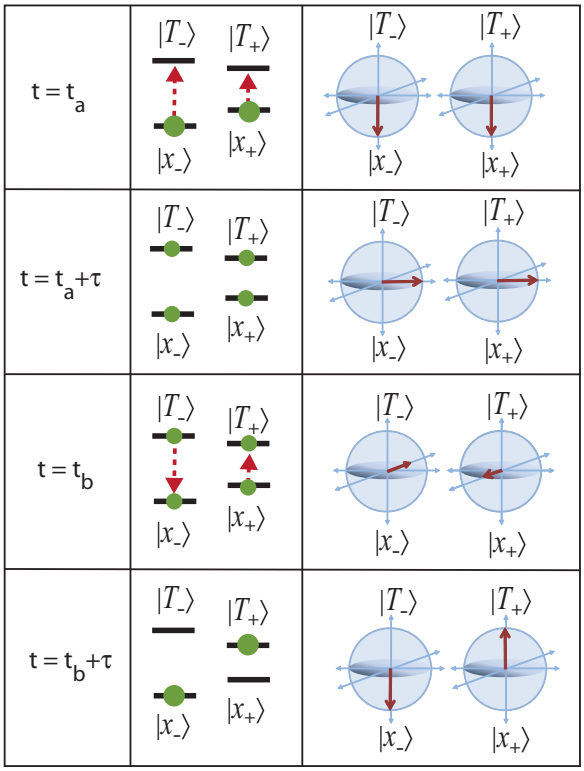

FIG. 3. (Color online) Visual representations of selective excitation of a spin-qubit state by two vertically polarized $\pi/2$ pulse area pulses. The middle column shows the probability of occupation of the four dot energy levels and the right column contains Bloch sphere representations of the two optically coupled, two-level systems. The top row shows a snapshot immediately before the first pulse, the second row immediately after the first pulse, the third row immediately before the second pulse, and the last row shows the dot in a state $\alpha e^{i\phi_\alpha}|x_-(t)\rangle + \beta e^{i\phi_\beta}|T_+(t)\rangle$ after the second pulse.

As a test of the validity of the assumptions made in this derivation, the exact equations of motion were solved numerically for two hyperbolic secant squared pulses with pulse area $\pi/2$ acting on a spin qubit state where $|\alpha| = |\beta|$. The delay was $\delta t = \pi/(\omega_{x_-T_-} - \omega_{x_+T_+}) + t_c$, where t_c was determined by graphical methods similar to Fig. 2(b). The pulses were tuned to $\omega_L = (\omega_{x_+T_+} + \omega_{x_-T_-})/2$, as in the discussion above, and the pulse bandwidth was about 2.5 times larger than $(\omega_{x_-T_-} - \omega_{x_+T_+})$. Neglecting decay and decoherence and assuming perfect polarization selectivity of the optical transitions, the fidelity (defined in Sec. IV) of the result of this numerical calculation when compared to the analytic result above is 0.9997.

III. PROPOSED EXPERIMENT

Here, we describe an experimental protocol that uses the excitation technique of Sec. II to create $|\psi^E(t)\rangle$, a precursor to spin-photon entanglement. We use four optical pulses to first create a coherent superposition of the qubit spin states and then selectively excite the $|x_+\rangle$ state to create state $|\psi^E(t)\rangle$. A fifth pulse measures the coherence of the created state, $|\psi^E(t)\rangle$,

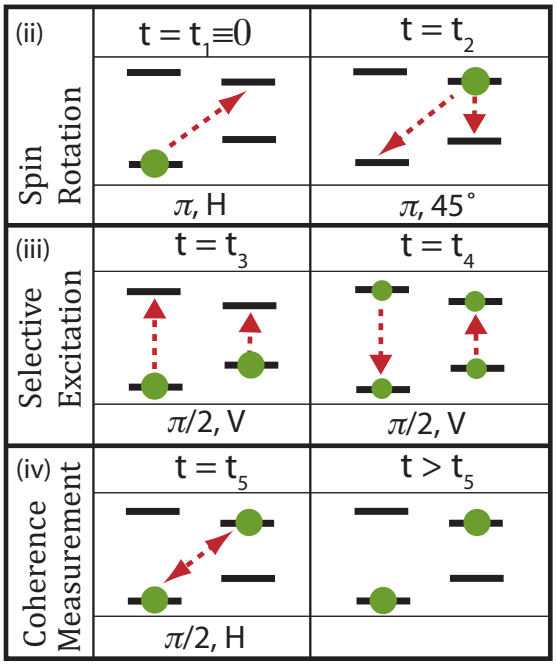

FIG. 4. (Color online) The proposed five-pulse sequence for creating $|\psi^E\rangle$ and measuring its coherence. The left column indicates the stage or function of the pulse(s) in that row, where stage (i) is initialization by the CW beam. In each panel the top label indicates the arrival time of the pulse at the dot, the arrows mark the transitions driven by the pulse, and the bottom label gives its polarization and pulse area. All pulses are on-resonance.

to demonstrate that the coherence of the spin superposition state was not destroyed during the selective excitation. The procedure can be thought of in four stages: (i) initialization to the spin ground state, $|\psi_{\rm init}(t)\rangle = e^{i\pi\Delta_e t}|x_-(t)\rangle$; (ii) spin rotation to $[-e^{i\pi(\Delta_h-\Delta_e)t_2}e^{i\pi\Delta_e t}|x_-(t)\rangle + ie^{i\pi(\Delta_h+\Delta_e)t_2}e^{-i\pi\Delta_e t}|x_+(t)\rangle]/\sqrt{2}$ as an example of the state of the spin qubit; (iii) selective excitation of the $|x_+\rangle$ state such that the final state is of the form $|\psi^E(t)\rangle = \alpha' e^{i\phi_\alpha}e^{i\pi\Delta_e t}|x_-(t)\rangle + \beta' e^{i\phi_\beta}e^{i\pi\Delta_h t}|T_+(t)\rangle$ including time dependence; and (iv) measurement of the coherence $\rho_{x_-T_+}$ present in this final state. Here the coherence $\rho_{x_-T_+}(t) = \langle x_-|\rho(t)|T_+\rangle = a^*_{x_-}(t)a_{T_+}(t)$ for a pure state, and ρ is the density matrix operator: $\rho \equiv |\psi\rangle\langle\psi|$. A CW laser resonant with the $|x_+\rangle$ to $|T_+\rangle$ transition initializes the dot to $|x_-\rangle$ by means of optical pumping. Steps (ii), (iii), and (iv) are pulse manipulations that are illustrated in Fig. 4. Note that this protocol (1) first rotates the spin to produce a qubit state that is a superposition of the states $|x_-\rangle$ and $|x_+\rangle$, (2) then selectively excites the $|x_+\rangle$ state to a trion state, and finally (3) measures the coherence associated with that excitation in three separate manipulations using five separate pulses, as described below.

A. Stage (i)—Initialization of the dot to a single eigenstate

Prior to optical initialization, the two spin states of the quantum dot $|x_-\rangle$ and $|x_+\rangle$ are in thermal equilibrium. We begin by initializing the dot to a single eigenstate before creating a coherent superposition state in stage (ii). It has been shown that a narrow bandwidth CW laser resonant with one transition (for instance, the $|x_+\rangle$ to $|T_+\rangle$ transition) will optically pump the spin to the ground state that is not coupled by the laser (in this case the $|x_-\rangle$ state).[51] (Tuning the CW beam to the $|x_-\rangle$ to $|T_-\rangle$ transition would similarly pump the spin to state $|x_+\rangle$. It is preferable to pump the $|x_+\rangle$ to $|T_+\rangle$ transition because its lower energy eliminates the possibility of exciting any nonradiative processes in the dot that could interact with the optical transitions.) Including the time-dependent phase as defined in the field interaction picture,[46] the initialized state is $|\Psi_{\rm init}(t)\rangle = e^{i\pi\Delta_e t}e^{i\phi_0}|x_-\rangle$, where $t = 0$ is defined as the arrival time of the first pulse [in stage (ii)]. ϕ_0 will be different each repetition period and will time-average to zero during detection, so it will be neglected in the following discussion.

The CW laser remains incident on the dot throughout the experiment. When the magnetic field is in the Voigt geometry, optical pumping occurs in a few trion radiative lifetimes, which is on the order of a few nanoseconds in this system.[50,51,53] Since the other manipulations are performed with a pulsed laser with a 13 ns repetition period, the dot is reinitialized after each five-pulse set. As such, each repetition period of the laser can be treated as an independent experiment (except for some memory remaining in the nuclear spins).

B. Stage (ii)—Spin rotation to create a coherent spin superposition

Once the dot is initialized to the state $|\psi_{\rm init}(t)\rangle$, we rotate the spin to

$$|\psi_2(t)\rangle = \frac{-1}{\sqrt{2}}e^{i\pi(\Delta_h-\Delta_e)t_2}e^{i\pi\Delta_e t}|x_-(t)\rangle + \frac{i}{\sqrt{2}}e^{i\pi(\Delta_h+\Delta_e)t_2}e^{-i\pi\Delta_e t}|x_+(t)\rangle.$$

$|\psi_2(t)\rangle$ is a nontrivial case of the arbitrary spin state $\alpha|x_-\rangle + \beta|x_+\rangle$ [or $|\psi_{\rm spin}(t)\rangle = \alpha' e^{i\pi\Delta_e t}|x_-(t)\rangle + \beta' e^{-i\pi\Delta_e t}|x_+(t)\rangle$ including time dependence], and is used as the initial state for selective excitation without loss of generality.

Although the spin rotation from the eigenstate $|x_-\rangle$ to an equal superposition of the electron spin (ground) states could be achieved using a single off-resonant Raman pulse,[6,7] combining this off-resonant pulse with the on-resonance pulses necessary for selective excitation in stage (iii) would require two pulsed lasers. Instead, we suggest a simple two-pulse sequence that achieves the effective spin rotation by way of a trion state intermediate, as shown in the first two frames of Fig. 4. This modification allows the entire sequence of five pulses required in this experiment to be produced by a single laser, because all pulses can have identical pulse widths and center frequencies.

Starting from the initialized state $|\psi_{\rm init}(t)\rangle = e^{i\pi\Delta_e t}e^{i\phi_0}|x_-\rangle$, first a horizontally polarized (H) pulse excites the system at $t = 0$. The pulse is short enough that its Fourier transform bandwidth covers all four optical transitions shown in Fig. 1. As in the previous section, due to the broad bandwidth, the pulses centered at ω_L can be approximated as on-resonance. Since only state $|x_-\rangle$ is occupied and the pulse is horizontally polarized, the pulse only couples states $|x_-\rangle$ and $|T_+\rangle$. The effect of resonant excitation of this two-level

system by the horizontally polarized electric field

$$\mathbf{E}_1(t) = E_1\hat{\mathbf{x}}\sqcap(t/\tau)\cos\omega t \tag{10}$$

is given in the field interaction picture by

$$\begin{bmatrix} c_{x_-}(\tau) \\ c_{T_+}(\tau) \end{bmatrix} = \begin{bmatrix} \cos\left(\frac{|\Omega_1|\tau}{2}\right) & i\sin\left(\frac{|\Omega_1|\tau}{2}\right) \\ i\sin\left(\frac{|\Omega_1|\tau}{2}\right) & \cos\left(\frac{|\Omega_1|\tau}{2}\right) \end{bmatrix} \begin{bmatrix} c_{x_-}(0) \\ c_{T_+}(0) \end{bmatrix}, \tag{11}$$

where $\Omega_1 = -\mu_{T_+x_-}E_1/\hbar$. If the pulse area $\Theta_1 = |\Omega_1|\tau$ is π, then the first pulse drives the system to $|T_+\rangle$ with unity probability, resulting in the state

$$|\psi_1(t)\rangle = ie^{i\pi\Delta_h t}|T_+(t)\rangle \text{ for } \tau < t < t_2. \tag{12}$$

Since $1/\tau \gg \Delta_e, \Delta_h$ for typical InAs dots, the pulses can be approximated as instantaneous when writing the phase accumulated between the pulses.

Next, a 45° polarized pulse, with equal horizontal and vertical components $E_x = E_y$, couples the $|T_+\rangle$ state to both ground states equally. For InAs dots, $\mu_{T_-x_-} = i\mu_{T_+x_-} = -\mu_{x_-T_-}$. Solving the equations of motion for the initial condition $|c_{T_+}(t_2)|^2 = 1$ gives

$$\begin{aligned} c_{x_-}(t_2+\tau) &= c_{T_+}(t_2)\frac{i}{\sqrt{2}}\sin\frac{|\Omega_2|\tau}{2}, \\ c_{x_+}(t_2+\tau) &= c_{T_+}(t_2)\frac{1}{\sqrt{2}}\sin\frac{|\Omega_2|\tau}{2}, \\ c_{T_+}(t_2+\tau) &= c_{T_+}(t_2)\cos\frac{|\Omega_2|\tau}{2}, \end{aligned} \tag{13}$$

where $\Omega_2 = -\mu_{T_+x_-}E_x/\hbar$. Therefore, if the second pulse has a pulse area $\Theta_2 = |\Omega_2|\tau$ of π, it will leave the dot in

$$\begin{aligned} |\psi_2(t)\rangle = [&-e^{i\pi(\Delta_h-\Delta_e)t_2}e^{i\pi\Delta_e t}|x_-(t)\rangle \\ &+ ie^{i\pi(\Delta_h+\Delta_e)t_2}e^{-i\pi\Delta_e t}|x_+(t)\rangle]/\sqrt{2} \\ &\text{for } t_2+\tau < t < t_3, \end{aligned} \tag{14}$$

which is of the form of $|\psi_{\text{spin}}(t)\rangle$ with $\alpha' = -e^{i\pi(\Delta_h-\Delta_e)t_2}/\sqrt{2}$ and $\beta' = ie^{i\pi(\Delta_h+\Delta_e)t_2}/\sqrt{2}$.

After the second pulse, the dot state is a coherent superposition of the electron spin states, which will precess due to the magnetic field until the next pulse arrives. This precession time contributes to the phases in Eq. (15), but the value of these phases is not critical for the use of state $|\psi_4(t)\rangle$ in the YLS proposal. The time delays between the first three pulses need not be precise, however they should be short to minimize decoherence and decay.

C. Stage (iii)—Selective excitation to $|\psi^E\rangle$

As derived in Sec. II, if the third and fourth pulses are vertically polarized with pulse area $\pi/2$, then the third pulse creates a coherent superposition of all four eigenstates. Between the third and fourth pulses, different phases accumulate for the two vertical transitions. If the delay between pulses is approximated as $\delta t = t_4 - t_3$ (neglecting the pulse width τ) and satisfies $\delta t = [2(\Delta_e+\Delta_h)]^{-1}$ and $(\delta t+\tau)\omega_L = \pi/2$, then pulses 3 and 4 will selectively excite the dot from $|\psi_2(t_3)\rangle$ to

$$\begin{aligned} |\psi_4(t)\rangle = {}&\alpha' ie^{i\pi\Delta_e t_3}e^{-\frac{i\pi\Delta_h}{2(\Delta_e+\Delta_h)}}e^{i\pi\Delta_e t}|x_-(t)\rangle \\ &-\beta' ie^{-i\pi\Delta_e t_3}e^{-\frac{i\pi\Delta_e}{2(\Delta_e+\Delta_h)}}e^{-i(\phi-\omega_L t_3)}e^{-i\pi\Delta_h t}|T_+(t)\rangle, \\ &t_4 < t < t_5, \end{aligned} \tag{15}$$

which has the form of $|\psi^E(t)\rangle$ with $\phi_\alpha = \frac{\pi(\Delta_e)}{2(\Delta_e+\Delta_h)} + \pi\Delta_e t_3$ and $\phi_\beta = \frac{-\pi\Delta_h}{2(\Delta_e+\Delta_h)} - \pi\Delta_e t_3$. Here we applied Eq. (7) with $t_a = t_3$, $t_b = t_4$, and $|\psi_2(t_3)\rangle$ providing the probability amplitudes $\mathbf{c}(t_3)$. Notice the phases of state $|\psi_4(t)\rangle$ continue to evolve in time after the fourth pulse. These phases are used in stage (iv) to measure the induced coherence $\rho_{x_-T_+}$, and they would not impair an entanglement procedure.

D. Readout

The CW beam, which also performs initialization, is used for readout. The readout signal is the detection of absorption of a photon by the final spin state due to the optical pumping back to the original spin state. The signal is measured by a square law detector that will detect a combination of the CW laser field ($\mathbf{E}_{\text{CW}}$) and the optical field radiated by the dot ($\mathbf{E}_S$). The destructive interference of these two fields appears as absorption.

The experimental techniques used to detect this small absorption affect the form of the detected signal, and thus require discussion here. Detection is nontrivial because the absorption signal is collinear with the incident lasers. Pulses are blocked by a polarizer such that they do not reach the detector. Modulation of the bias voltage across the sample translates to a modulated Stark shift in the dot. This voltage modulation can be used as the reference frequency for phase-sensitive detection with a lock-in amplifier, which greatly improves the signal-to-noise ratio of the readout.[54] The CW beam is on-resonance with the $|x_+\rangle$ to $|T_+\rangle$ transition, such that $\mathbf{E}_{\text{CW}} = \hat{\mathbf{y}}E_{\text{CW}}\cos\omega_{T_+x_+}t$. Due to the phase-sensitive detection, only terms proportional to $\frac{1}{T}\int_0^{0+T}(\mathbf{E}_{\text{CW}}\cdot\mathbf{E}_S)dt$, where T is the repetition period of the pulsed laser, will be detected by the lock-in since only $\mathbf{E}_S$ is modulated. Because the CW field also optically pumps the system back to a single eigenstate within a few trion lifetimes, we assume the laser repetition period is sufficiently long such that the system is reinitialized between pulse sequences.

Since the signal is measured by homodyning with the classical probe field, the signal depends only on the average dipole moment of the dot. We use a semiclassical, density matrix approach to calculate this quantity.[46] Therefore,

$$\mathbf{E}_S(t) = K[\boldsymbol{\mu}_{x_+T_+}\rho_{T_+x_+}(t) - \boldsymbol{\mu}_{T_+x_+}\rho_{x_+T_+}(t)], \tag{16}$$

where K is a (complex) constant, $\mu_{x_+T_+}$ is the dipole moment between states $|x_+\rangle$ and $|T_+\rangle$, and $\rho_{x_+T_+}$ is the off-diagonal density matrix element representing the optical dipole induced coherence in the Schrödinger picture, $\rho_{x_+T_+}(t) = a_{x_+}(t)a^*_{T_+}(t) = c_{x_+}(t)c^*_{T_+}(t)e^{i\omega_L t}$. The field interaction picture is convenient for derivations, but it is necessary to translate back to the Schrödinger picture to calculate expectation values of observable quantities.

Given that the decay of state $|T_+\rangle$ strongly affects the coherence between states $|T_+\rangle$ and $|x_+\rangle$, this coherence is best calculated in the density matrix picture.[46] It is a good approximation that the CW laser only couples states $|x_+\rangle$ and $|T_+\rangle$, due to the very narrow bandwidth of frequency-stabilized CW lasers. The density matrix equations for the four-level system with excitation by the CW beam and decay can be solved analytically for the coherence $\rho_{T_+x_+}$ under the condition

that the optical pumping rate is much faster than the repetition rate of the laser. The result is that the detected readout signal is proportional to $\rho_{T_+T_+}(t_f)/2 + \rho_{T_-T_-}(t_f)/2 + \rho_{x_+x_+}(t_f)$, where $\rho_{ii}(t_f)$ is the occupation probability of state $|i\rangle$ immediately after the final pulse. (For the full five-pulse experiment illustrated in Fig. 4, $t_f = t_5$.) This result can be understood intuitively since a dot in state $|x_+\rangle$ absorbs the CW beam, while a dot in state $|x_-\rangle$ does not. Furthermore, a dot excited to either state $|T_+\rangle$ or state $|T_-\rangle$ has a 50% chance of decaying into state $|x_+\rangle$ where it is measured by the CW beam.

Because this readout method involves leaving the CW beam on during the pulse manipulations, the effect of the CW beam on the dot during this manipulation time, $t_5 - t_1 = t_5$, must be considered. However, as long as the CW Rabi frequency is much smaller than $1/t_5$, its effect on the dot during the pulse sequence will be small. The effect of the CW beam on the fidelity of the proposed pulse manipulations is addressed with numerical simulations in Sec. IV.

E. Stage (iv)—Coherence measurement

Measuring the induced coherence $\rho_{x_-T_+}$ following the creation of $|\psi^E(t)\rangle = [\alpha' e^{i\phi_\alpha} e^{i\pi\Delta_e t}|x_-(t)\rangle + \beta' e^{i\phi_\beta} e^{i\pi\Delta_h t}|T_+(t)\rangle]$ is essential for a demonstration of entanglement. As derived in the preceding section, the experimentally measured signal detects populations. However, a horizontally polarized pulse with pulse area $\pi/2$ can rotate the coherence associated with $|\psi^E(t)\rangle$, $\rho_{x_-T_+}(t)$, into a population that can be measured by the CW laser.[55] The addition of a phase-stable, fifth on-resonance pulse enables the observation of optical Ramsey fringes due to the relative phase accumulated after pulse 4 by state $|x_-\rangle$ relative to state $|T_+\rangle$.

The state of the system after the fourth pulse [given by Eq. (15)] can be written as $\mathbf{c}(t_4+\tau)$ with $c_{x_+}(t_4+\tau) = c_{T_-}(t_4+\tau) = 0$, and therefore

$$\begin{bmatrix} c_{x_-}(t_5+\tau) \\ c_{T_+}(t_5+\tau) \end{bmatrix} = \begin{bmatrix} \cos\left(\frac{\theta_5}{2}\right) & ie^{i\phi_5}\sin\left(\frac{\theta_5}{2}\right) \\ ie^{-i\phi_5}\sin\left(\frac{\theta_5}{2}\right) & \cos\left(\frac{\theta_5}{2}\right) \end{bmatrix} \times \begin{bmatrix} e^{\pi i\Delta_e(t_5-t_4)} & 0 \\ 0 & e^{\pi i\Delta_h(t_5-t_4)} \end{bmatrix} \begin{bmatrix} c_{x_-}(t_4+\tau) \\ c_{T_+}(t_4+\tau) \end{bmatrix}, \tag{17}$$

where $\theta_5 = |\Omega_5|\tau$ and $\Omega_5 = |\Omega_5|e^{-i\phi_5}$. Again, terms of order $\Delta_e\tau$ are neglected. Using the result from the preceding section, the measured signal after the proposed fifth pulse with Ω_5 real and $\Omega_5\tau = \pi/2$ is proportional to

$$\begin{aligned} &\tfrac{1}{2}\rho_{T_+T_+}(t_5+\tau) + \tfrac{1}{2}\rho_{T_-T_-}(t_5+\tau) + \rho_{x_+x_+}(t_5+\tau) \\ &\quad = \tfrac{1}{4}\rho_{x_-x_-}(t_4+\tau) + \tfrac{1}{4}\rho_{T_+T_+}(t_4+\tau) \\ &\qquad + \tfrac{1}{2}\mathrm{Im}[\rho_{x_-T_+}(t_4+\tau)e^{i\omega_{x_-T_+}(t_5-t_4)/2}]. \end{aligned} \tag{18}$$

This is calculated by combining Eq. (3), Eq. (17), and the definition $\rho_{ij} = a_i a_j^*$ (where a_i is a probability amplitude in the Schrödinger, rather than field interaction, representation). Therefore, the coherence $\rho_{x_-T_+}(t_4+\tau)$ of $|\Psi^E\rangle$ after pulse 4 can be measured by varying the delay between pulses 4 and 5 (provided this delay is phase-stable on the scale of $\omega_{x_-T_+}$). The coherence $\rho_{x_-T_+}(t_4+\tau)$ is proportional to the amplitude of the oscillation of the CW absorption as a function of this delay (Fig. 5).

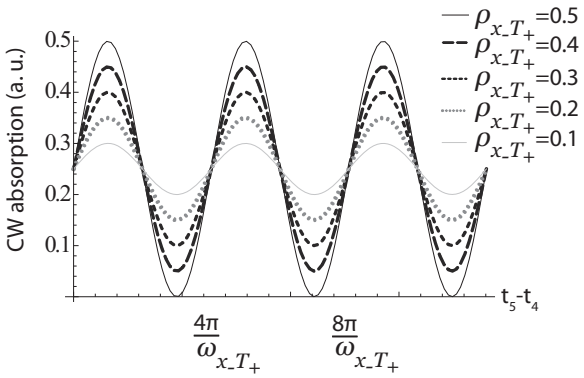

FIG. 5. A plot of the CW absorption readout signal after the fifth pulse, given by Eq. (18), for several values of $\rho_{x_-T_+}$. The plot assumes $\rho_{x_-x_-}(t_4+\tau) = \rho_{T_+T_+}(t_4+\tau) = 0.5$ after the fourth pulse. The amplitude of the oscillation is proportional to the coherence $\rho_{x_-T_+}$.

IV. FIDELITY FROM NUMERICAL SIMULATIONS

In this section, numerical solutions to the density matrix equations using realistic experimental parameters (including more realistic pulse shapes) are compared to the analytic results obtained in the previous sections. A finite pulse bandwidth, which does not couple all four transitions equally, minor temporal overlap of the pulses, trion state decay, decoherence, spin flips and the effect of the CW beam during and between the pulses are all possible causes of differences between analytical and numerical results. We quantify the effect of these deviations by calculating the fidelity between the analytically calculated and simulated final state of the dot.

A quantum transformation can be characterized by its fidelity F defined as

$$F = \overline{|\langle\psi|U_A^\dagger U_I|\psi\rangle|}, \tag{19}$$

where U_I is the ideal unitary operator for the transformation, U_A is the operator of the actual (calculated, simulated, or measured) transformation, and the overbar indicates an average over all possible initial states.[56] Fidelity can be alternately defined as

$$F(\rho_I,\rho_A) = \mathrm{Tr}\sqrt{\rho_I\rho_A} \tag{20}$$

to include decay and decoherence.[57]

This section calculates the fidelity $F(\rho_{\mathrm{theory}},\rho_{\mathrm{sim}})$ to compare the simulated result of the suggested experiment to the ideal, theoretical result. As presented in the previous sections, the theoretical calculation consists of 4×4 transfer matrices in the probability amplitude picture; each matrix corresponds to either the action of a pulse or the time dependence of the states between pulses. The simulations are numerical solutions to the coupled equations of motion for the states of the dot in the density matrix picture, which allows decay and decoherence to be included.[46]

A numerical simulation with hyperbolic secant squared pulse shapes, 1.9 ps pulse widths [full width at half-maximum

(FWHM) power], a dipole moment for all four optical transitions of 6.75 D, $\Delta_e = 30$ GHz, $\Delta_h = 20$ GHz, and no decay or decoherence agrees with the transfer matrix calculation for the effect of pulses 1 through 4 with a fidelity of 0.999. Including in the simulation a trion decay rate of 1.17×10^9 s^{-1}, no pure dephasing of the optical transitions, equal electron and hole spin-flip rates of 6.28×10^6 s^{-1}, and 2.51×10^8 s^{-1} pure electron spin dephasing only degrades the fidelity to 0.991. This is a small change because decay and decoherence only reduce the fidelity during the pulse sequence, and the total time required for the entire four-pulse sequence is only 25 ps. It is because the effects of decay and decoherence are so small that we could present the pulse manipulations in the amplitude picture and neglect decay. Including a CW beam with an incident intensity of 2.5×10^6 W/m^2, such as would be used for initialization and readout, has only a small effect on the fidelity, lowering it by only 0.002 to 0.989. The values used above and plotted as the highlighted point in Fig. 6(c) are estimates of realistic values for InAs quantum dots,[53,58–60] but values can vary from dot to dot and certainly could be quite different in other qubit systems, for example trapped ions. The hole spin-flip rate is likely exaggerated here, but even with these values it has a negligible ($\leqslant$0.002) effect on both the fidelity and the entropy of entanglement discussed below. Figure 6 shows the effect that different trion decay, trion decoherence, and spin-flip times would have on the fidelity (shown by the blue diamonds).

The selective excitation pulse pair, pulses 3 and 4, could be replaced by a single narrow bandwidth pulse that only excites the $|x_+\rangle$ to $|T_+\rangle$ transition. This seems like a simpler approach, but a pulse that is narrow enough to only excite a single transition is also long enough to suffer fidelity degradation from decay and decoherence. A pulse with a power FWHM of 12 ps achieves the highest fidelity possible for single pulse selective excitation, which is 0.995 for the decay and decoherence values from the preceding paragraph. This single pulse operation is 30 ps long, if we define the length of the operation as the time interval between the 5% power point on the leading edge of the first pulse and the 5% power point on the falling edge of the final pulse. For comparison, the two selective excitation pulses, pulses 3 and 4 from the experiment proposed in Sec. III, have an operation time of only 14 ps, and a fidelity of 0.998. Therefore, two phase-locked pulses selectively excite the dot in a shorter time compared to a single narrow bandwidth pulse, while achieving a similar fidelity. The method of selective excitation with two phase-locked pulses (explained in detail in Sec. II) is essential if the available lasers cannot directly generate pulses with sufficiently narrow bandwidths to use the single pulse method and do not have enough power to narrow the bandwidth through simple spectral filtering. As an example of the limitation of long, narrow bandwidth pulses, a 200 ps pulse such as could be created by a high-speed electro-optic modulator is simulated to have a best-case fidelity of 0.897, largely due to decay and decoherence.

Recall that the eventual goal is to create state $|\Psi^E(t)\rangle$ in a cavity, such that upon radiative decay, entanglement is created between the electron spin and the presence of a photon in the cavity mode. Assuming the cavity completely suppresses all radiative decay that would create horizontally

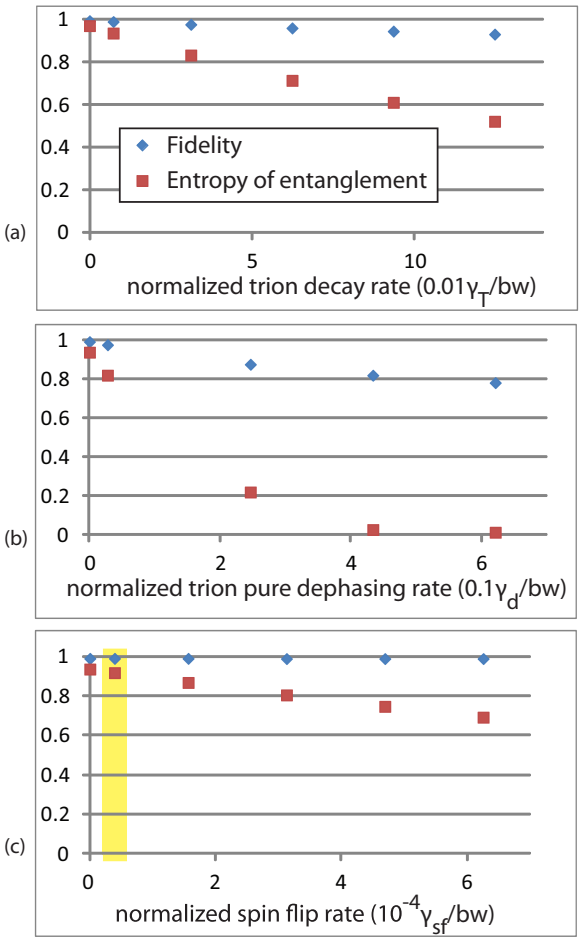

FIG. 6. (Color online) Fidelity (blue diamonds) and entropy of entanglement (red squares) for several rates of trion decay (a), pure dephasing of the ground to trion state (optical) transitions (b), and spin flips (c), all in the presence of a CW beam with an incident intensity of 2.5×10^6 W/m^2. All rates are normalized to the pulse bandwidth (bw) of 1.6×10^{11} s^{-1}. Plot (a) includes decoherence, but zero pure dephasing of the optical transitions. Electron and hole spin flips and spin pure dephasing are set to zero for plots (a) and (b). In plots (b) and (c), the trion decay rate is a constant 1.17×10^9 s^{-1}. Plot (c) requires that the electron and hole spin-flip rates are equal and that both electron and hole spin pure dephasing is zero. Plot (c) again assumes zero trion pure dephasing. The highlighted points in plot (c) mark an electron and hole spin-flip rate of 6.28×10^6 s^{-1} and represent a realistic estimate of the fidelity and entropy of entanglement for InAs quantum dots based on previously measured decay and decoherence rates.[53,58–60]

polarized photons and assuming all excited states decay and emit photons before decoherence can alter the state of the dot, the state of the system after radiative decay would be given by the following mapping:

$$\begin{aligned} |x+\rangle|0\rangle_c &\rightarrow |x+\rangle|0\rangle_c, \\ |x-\rangle|0\rangle_c &\rightarrow |x-\rangle|0\rangle_c, \\ |t+\rangle|0\rangle_c &\rightarrow |x+\rangle|1\rangle_c, \\ |t-\rangle|0\rangle_c &\rightarrow |x-\rangle|1\rangle_c. \end{aligned} \tag{21}$$

With these assumptions, $|\Psi^E\rangle$ would decay to $[e^{i\Phi_\alpha}e^{i\pi\Delta_e t}|x_-(t)\rangle|0\rangle_c + e^{i\Phi_\beta}e^{-i\pi\Delta_e t}|x_+(t)\rangle|1\rangle_c]/\sqrt{2}$. For simplicity, the calculations below assume $\Phi_\alpha = \phi_\alpha$ and $\Phi_\beta = \phi_\beta$.

Entropy of entanglement is a method of quantifying the entanglement of a state that exists in a composite Hilbert space.[61] The state $[e^{i\Phi_\alpha}e^{i\pi\Delta_e t}|x_-(t)\rangle|0\rangle_c + e^{i\Phi_\beta}e^{-i\pi\Delta_e t}|x_+(t)\rangle|1\rangle_c]/\sqrt{2}$ has maximum entanglement between the electron spin and the presence or absence of a photon in the cavity mode, and thus has an entropy of entanglement of 1. The numerical simulations described above produce a density matrix that describes how well the proposed scheme of optical pulses creates $|\psi^E\rangle$. This has been quantified as a fidelity, but it would be more relevant to quantify how much entanglement would be created if the simulated state were to decay in a cavity. After applying the mapping above to the simulated density matrix, a procedure presented by Wootters gives the entropy of entanglement of the spin-photon system, even if the simulation results in a mixed case for the density matrix.[62]

Figure 6 plots the entropy of entanglement (red squares) in addition to the fidelity (blue diamonds) for various parameters. It is important to consider the entropy of entanglement and not simply the fidelity of the process, as shown in Fig. 6(a), where the fidelity is barely affected by the increased decay yet the entropy of entanglement drops nearly to 0.5. Figure 6(b) shows the degradation of the entropy of entanglement by pure dephasing of the optical transition, a type of decoherence. Figure 6(b) illustrates the importance of coherence between the trion states and the ground states for the creation of entanglement, demonstrating why the measurement of coherence in stage (iv) is essential.

The expected entropy of entanglement using the typical parameters for InAs dots stated above and including the effect of the CW beam is 0.915 [plotted as the highlighted point in Fig. 6(c)]. This is the amount of entanglement, out of a maximum of 1, that the proposed pulse scheme is expected to create between the electron spin in a typical InAs quantum dot and the existence of a photon, if the dot were allowed to decay in a cavity. The CW laser could be gated off after initialization to achieve a fidelity of 0.991 and an entropy of 0.929. As illustrated by Fig. 6, the entropy of entanglement is primarily limited by the trion decay rate and to a lesser extent by the electron spin-flip rate. (We are assuming a dot with zero optical pure dephasing.) Shorter pulses and a higher magnetic field would reduce the delay between pulses and thus the effects of decay, decoherence, and spin flips, however the pulse bandwidth must be kept small enough that higher-energy dot states are not excited. Using a detuned pulse that adiabatically eliminates the trion state to accomplish the spin rotation [stage (iv) in Fig. 4] would likely provide further improvement of the fidelity and entropy of entanglement by reducing the impact of trion decay during stage (ii).

V. CONCLUSIONS

We presented an experimental design involving a sequence of four pulses which demonstrates the coherent optical excitation of a spin qubit to a state of the form $|\psi^E(t)\rangle = \alpha' e^{i\phi_\alpha}e^{i\pi\Delta_e t}|x_-(t)\rangle + \beta' e^{i\phi_\beta}e^{i\pi\Delta_h t}|T_+(t)\rangle$, where α' and β' are complex numbers of magnitude $1/\sqrt{2}$. A proposed fifth pulse demonstrates the ability to perform measurements on the created state by measuring its coherence. Numerical simulations with experimentally relevant parameters predict high fidelities for the proposed experiment. If the ideal coherent superposition state $|\psi^E\rangle$ were created in a dot in an appropriate optical cavity, the state of the dot-cavity system would be $|\Psi^E\rangle = |\psi^E\rangle|0\rangle_c$, and it would decay deterministically to the state $\alpha' e^{i\Phi_\alpha}e^{i\pi\Delta_e t}|x_-(t)\rangle|0\rangle_c + \beta' e^{i\Phi_\beta}e^{-i\pi\Delta_e t}|x_+(t)\rangle|1\rangle_c$, which possesses maximal entanglement between the electron spin and the occupation of the cavity mode. Realistic values for InAs dots predict an actual entropy of entanglement of 0.929. Thus, this experimental proposal represents a preliminary step toward the deterministic entanglement of a photon and a spin in a quantum dot.

ACKNOWLEDGMENTS

This work was supported by NSF, ARO, DARPA, and AFOSR.

*Present address: Laboratory of Chemical Physics, National Institute of Diabetes and Digestive and Kidney Diseases, National Institutes of Health, Bethesda, MD 20892-0520, USA.
†dst@umich.edu

[1] A. J. Ramsay, Semicond. Sci. Technol. **25**, 103001 (2010).
[2] S. C. Benjamin, B. W. Lovett, and J. M. Smith, Laser Photon. Rev. **3**, 556 (2009).
[3] R. J. Warburton, Nat. Mater. **12**, 483 (2013).
[4] C.-M. Simon, T. Belhadj, B. Chatel, T. Amand, P. Renucci, A. Lemaitre, O. Krebs, P. A. Dalgarno, R. J. Warburton, X. Marie, and B. Urbaszek, Phys. Rev. Lett. **106**, 166801 (2011).
[5] S. J. Boyle, A. J. Ramsay, A. M. Fox, and M. S. Skolnick, Physica E **42**, 2485 (2010).
[6] D. Press, T. D. Ladd, B. Zhang, and Y. Yamamoto, Nature (London) **456**, 218 (2008).
[7] E. D. Kim, K. Truex, X. Xu, B. Sun, D. G. Steel, A. S. Bracker, D. Gammon, and L. J. Sham, Phys. Rev. Lett. **104**, 167401 (2010).
[8] D. Press, K. De Greve, P. L. McMahon, T. D. Ladd, B. Friess, C. Schneider, M. Kamp, S. Hofling, A. Forchel, and Y. Yamamoto, Nat. Photon. **4**, 367 (2010).
[9] K. De Greve *et al.*, Nat. Phys. **7**, 872 (2011).
[10] T. M. Godden, J. H. Quilter, A. J. Ramsay, Y. Wu, P. Brereton, S. J. Boyle, I. J. Luxmoore, J. Puebla-Nunez, A. M. Fox, and M. S. Skolnick, Phys. Rev. Lett. **108**, 017402 (2012).
[11] E. Poem, Y. Kodriano, C. Tradonsky, N. H. Lindner, B. D. Gerardot, P. M. Petroff, and D. Gershoni, Nat. Phys. **6**, 993 (2010).
[12] L. A. Larsson, E. S. Moskalenko, and P. O. Holtz, Appl. Phys. Lett. **98**, 071906 (2011).
[13] Y. Kodriano, I. Schwartz, E. Poem, Y. Benny, R. Presman, T. A. Truong, P. M. Petroff, and D. Gershoni, Phys. Rev. B **85**, 241304 (2012).
[14] K. Muller, T. Kaldewey, R. Ripszam, J. S. Wildmann, A. Bechtold, M. Bichler, G. Koblmueller, G. Abstreiter, and J. J. Finley, Sci. Rep. **3**, 1906 (2013).

[15]F. Klotz, V. Jovanov, J. Kierig, E. C. Clark, D. Rudolph, D. Heiss, M. Bichler, G. Abstreiter, M. S. Brandt, and J. J. Finley, Appl. Phys. Lett. **96**, 053113 (2010).
[16]A. J. Bennett, M. A. Pooley, Y. M. Cao, N. Skold, I. Farrer, D. A. Ritchie, and A. J. Shields, Nat. Commun. **4**, 1522 (2013).
[17]J. Beyer, P. H. Wang, I. A. Buyanova, S. Suraprapapich, C. W. Tu, and W. M. Chen, J. Phys.: Condens. Matter **24**, 145304 (2012).
[18]Y. Benny, Y. Kodriano, E. Poem, D. Gershoni, T. A. Truong, and P. M. Petroff, Phys. Rev. B **86**, 085306 (2012).
[19]V. Jovanov, S. Kapfinger, M. Bichler, G. Abstreiter, and J. J. Finley, Phys. Rev. B **84**, 235321 (2011).
[20]J. Beyer, I. A. Buyanova, S. Suraprapapich, C. W. Tu, and W. M. Chen, Appl. Phys. Lett. **98**, 203110 (2011).
[21]C.-Y. Lu, Y. Zhao, A. N. Vamivakas, C. Matthiesen, S. Falt, A. Badolato, and M. Atature, Phys. Rev. B **81**, 035332 (2010).
[22]E. Poem, Y. Kodriano, C. Tradonsky, B. D. Gerardot, P. M. Petroff, and D. Gershoni, Phys. Rev. B **81**, 085306 (2010).
[23]K. Konthasinghe, M. Peiris, Y. Yu, M. F. Li, J. F. He, L. J. Wang, H. Q. Ni, Z. C. Niu, C. K. Shih, and A. Muller, Phys. Rev. Lett. **109**, 267402 (2012).
[24]C. Tonin, R. Hostein, V. Voliotis, R. Grousson, A. Lemaitre, and A. Martinez, Phys. Rev. B **85**, 155303 (2012).
[25]K. Asakura, Y. Mitsumori, H. Kosaka, K. Edamatsu, K. Akahane, N. Yamamoto, M. Sasaki, and N. Ohtani, Phys. Rev. B **87**, 241301 (2013).
[26]J. D. Mar, J. J. Baumberg, X. L. Xu, A. C. Irvine, C. R. Stanley, and D. A. Williams, Phys. Rev. B **87**, 155315 (2013).
[27]D. Heiss, V. Jovanov, F. Klotz, D. Rudolph, M. Bichler, G. Abstreiter, M. S. Brandt, and J. J. Finley, Phys. Rev. B **82**, 245316 (2010).
[28]A. N. Vamivakas, C.-Y. Lu, C. Matthiesen, Y. Zhao, S. Falt, A. Badolato, and M. Atature, Nature (London) **467**, 297 (2010).
[29]J. R. Schaibley, A. P. Burgers, G. A. McCracken, D. G. Steel, A. S. Bracker, D. Gammon, and L. J. Sham, Phys. Rev. B **87**, 115311 (2013).
[30]D. P. DiVincenzo, Fortschr. Phys. **48**, 771 (2000).
[31]A. Greilich, S. G. Carter, D. Kim, A. S. Bracker, and D. Gammon, Nat. Photon. **5**, 703 (2011).
[32]K. Muller, G. Reithmaier, E. C. Clark, V. Jovanov, M. Bichler, H. J. Krenner, M. Betz, G. Abstreiter, and J. J. Finley, Phys. Rev. B **84**, 081302 (2011).
[33]K. Muller, A. Bechtold, C. Ruppert, C. Hautmann, J. S. Wildmann, T. Kaldewey, M. Bichler, H. J. Krenner, G. Abstreiter, M. Betz, and J. J. Finley, Phys. Rev. B **85**, 241306 (2012).
[34]W. Liu, A. S. Bracker, D. Gammon, and M. F. Doty, Phys. Rev. B **87**, 195308 (2013).
[35]K. Muller *et al.*, Ann. Phys. **525**, 49 (2013).
[36]F. Schlosser, A. Knorr, S. Mukamel, and M. Richter, New J. Phys. **15**, 025004 (2013).
[37]D. Kim, S. G. Carter, A. Greilich, A. S. Bracker, and D. Gammon, Nat. Phys. **7**, 223 (2011).
[38]J. I. Cirac, P. Zoller, H. J. Kimble, and H. Mabuchi, Phys. Rev. Lett. **78**, 3221 (1997).
[39]L.-M. Duan, A. Kuzmich, and H. J. Kimble, Phys. Rev. A **67**, 032305 (2003).
[40]W. Yao, R. B. Liu, and L. J. Sham, Phys. Rev. Lett. **95**, 030504 (2005).
[41]K. De Greve *et al.*, Nature (London) **491**, 421 (2012).
[42]W. B. Gao, P. Fallahi, E. Togan, J. Miguel-Sanchez, and A. Imamoglu, Nature (London) **491**, 426 (2012).
[43]J. R. Schaibley, A. P. Burgers, G. A. McCracken, L. M. Duan, P. R. Berman, D. G. Steel, A. S. Bracker, D. Gammon, and L. J. Sham, Phys. Rev. Lett. **110**, 167401 (2013).
[44]E. M. Purcell, Phys. Rev. **69**, 681 (1946).
[45]J.-M. Gerard and B. Gayral, J. Lightwave Technol. **17**, 2089 (1999).
[46]P. R. Berman and V. S. Malinovsky, *Principles of Laser Spectroscopy and Quantum Optics*, 1st ed. (Princeton University Press, Princeton, NJ, 2011).
[47]Pulse area $\equiv \int_{-\infty}^{\infty} \Omega(t')\, dt'$.
[48]C. Piermarocchi, P. Chen, Y. S. Dale, and L. J. Sham, Phys. Rev. B **65**, 075307 (2002).
[49]L. A. Webster, K. Truex, L. M. Duan, D. G. Steel, A. S. Bracker, D. Gammon, and L. J. Sham (unpublished).
[50]C. Emary, X. Xu, D. G. Steel, S. Saikin, and L. J. Sham, Phys. Rev. Lett. **98**, 047401 (2007).
[51]X. Xu, Y. Wu, B. Sun, Q. Huang, J. Cheng, D. G. Steel, A. S. Bracker, D. Gammon, C. Emary, and L. J. Sham, Phys. Rev. Lett. **99**, 097401 (2007).
[52]E. D. Kim, Ph.D. thesis, University of Michigan, 2009.
[53]E. D. Kim, K. Truex, A. Amo, X. Xu, D. G. Steel, A. S. Bracker, D. Gammon, and L. J. Sham, Appl. Phys. Lett. **97**, 113110 (2010).
[54]B. Alen, F. Bickel, K. Karrai, R. J. Warburton, and P. M. Petroff, Appl. Phys. Lett. **83**, 2235 (2003).
[55]C. P. Slichter, *Principles of Magnetic Resonance* (Springer, New York, 1996).
[56]J. F. Poyatos, J. I. Cirac, and P. Zoller, Phys. Rev. Lett. **78**, 390 (1997).
[57]M. A. Nielsen and I. L. Chuang, *Quantum Computation and Quantum Information*, 1st ed. (Cambridge University Press, Cambridge, UK, 2000).
[58]X. Xu, B. Sun, E. D. Kim, K. Smirl, P. R. Berman, D. G. Steel, A. S. Bracker, D. Gammon, and L. J. Sham, Phys. Rev. Lett. **101**, 227401 (2008).
[59]X. Xu, B. Sun, P. R. Berman, D. G. Steel, A. S. Bracker, D. Gammon, and L. J. Sham, Nat. Phys. **4**, 692 (2008).
[60]X. Xu, W. Yao, B. Sun, D. G. Steel, A. S. Bracker, D. Gammon, and L. J. Sham, Nature (London) **459**, 1105 (2009).
[61]C. H. Bennett, H. J. Bernstein, S. Popescu, and B. Schumacher, Phys. Rev. A **53**, 2046 (1996).
[62]W. K. Wootters, Phys. Rev. Lett. **80**, 2245 (1998).